

Possibilities of direct production of superheavy nuclei with $Z=112-118$ in different evaporation channels

J. Hong,

*Department of Physics and Institute of Physics and Applied Physics,
Yonsei University, Seoul 03722, Korea*

G. G. Adamian,

Joint Institute for Nuclear Research, Dubna 141980, Russia

N. V. Antonenko,

*Joint Institute for Nuclear Research, Dubna 141980, Russia
Tomsk Polytechnic University, 634050 Tomsk, Russia*

P. Jachimowicz,

*Institute of Physics, University of Zielona Góra,
Szafrana 4a, 65516 Zielona Góra, Poland*

M. Kowal*

*National Centre for Nuclear Research,
Pasteura 7, 02-093 Warsaw, Poland*

(Dated: March 17, 2024)

Abstract

The production cross sections of heaviest isotopes of superheavy nuclei with charge numbers 112–118 are predicted in the $xn-$, $pxn-$, and $\alpha xn-$ evaporation channels of the ^{48}Ca -induced complete fusion reactions for future experiments. The estimates of synthesis capabilities are based on a uniform and consistent set of input nuclear data. Nuclear masses, deformations, shell corrections, fission barriers and decay energies are calculated within the macroscopic-microscopic approach for even-even, odd- Z and odd- N nuclei. For odd systems the blocking procedure is used. To find, the ground states via minimisation and saddle points using Immersion Water flow technique, multidimensional deformation spaces, containing non-axiality are used. As shown, current calculations based on a new set of mass and barriers, agree very well with experimentally known cross-sections, especially in the $3n$ -evaporation channel. The dependencies of these predictions on the mass/fission barriers tables and fusion models are discussed. A way is shown to produce directly unknown superheavy isotopes in the $1n-$ or $2n-$ evaporation channels. The synthesis of new superheavy isotopes unattainable in reactions with emission of neutrons is proposed in the promising channels with emission of protons ($\sigma_{pxn} \simeq 10 - 200 \text{ fb}$) and alphas ($\sigma_{\alpha xn} \simeq 5 - 500 \text{ fb}$).

PACS numbers: 25.70.Hi, 24.10.-i, 24.60.-k

Key words: Superheavy nuclei; Complete fusion reactions; Production of new isotopes; Superheavy nuclei; $xn-$, $pxn-$, and αxn -evaporation channels

*Electronic address: michal.kowal@ncbj.gov.pl

I. INTRODUCTION

The production and spectroscopic study of superheavy nuclei (SHN) is currently one of the important topics in nuclear experiment and theory. Due to the extremely short lifetimes of SHN and the exceptionally low probabilities of their production the final cross-sections are extremely small. Although determine them is a huge challenge for today theory, only having reached this stage it will be possible to make reliable predictions of probabilities for synthesis even heavier, still non-existent SHN. The ^{48}Ca -induced complete fusion reactions have been successfully used to synthesize SHN with the charge numbers $Z=112$ – 118 in the neutron evaporation channels (xn -evaporation channels) [1–11] and to approach to "the island of stability" of SHN predicted at $Z=114$ – 126 and neutron numbers $N=172$ – 184 by the nuclear shell models [12–15]. The most of these SHN have been obtained in the $3n$ - and $4n$ -evaporation channels. Only in the reactions $^{48}\text{Ca}+^{242}\text{Pu}$, $^{48}\text{Ca}+^{243}\text{Am}$, and $^{48}\text{Ca}+^{245}\text{Cm}$ the evaporation residues have been detected in the $2n$ -evaporation channel. The nuclei $^{285,287}\text{Fl}$ and ^{292}Ts have been also produced in the $5n$ -evaporation channel. On the agenda is to expand the region of SHN in the direction of the magic neutron number $N = 184$, the center of the predicted "island of stability". For this purpose, we should study both new experimental possibilities and possible reaction channels. New isotopes of heaviest nuclei with $Z=112$ – 117 can be synthesized in the ^{48}Ca -induced actinide-based complete fusion-evaporation reactions with the emission of charged particle (proton " p " or alpha-particle " α ") and neutron(s) from the compound nucleus (CN). Note that the possibility of the production of new heaviest isotopes of superheavy nuclei with charge numbers 113, 115, and 117 in the proton evaporation channels with rather high efficiency was suggested for the first time in Ref. [16]. This extremely intriguing suggestion was tested in Refs. [17] and [18].

One can also observe new isotopes in the $1n$ - and $2n$ -evaporation channels of the ^{48}Ca -induced actinide-based complete fusion reactions. Using the predictions of superheavy nuclei properties of Ref. [19], we have recently studied these possibilities in Refs. [17, 20]. We have revealed how rapidly the evaporation residue cross section decreases with decreasing beam energy in the sub-barrier region.

An interesting question is how the estimation of production cross sections change if we replace the mass table containing the predictions of SHN properties. Taking other mass table, we should incorporate it in all steps of the calculation of the evaporation residue cross sec-

tions. As known, the evaporation residue cross sections depend on the capture cross section, fusion probability (formation of the CN), and survival probability (the survival with respect to fission). The last one seems to be the most sensitive to the SHN properties. However, the fusion probability also crucially depends on the change of the mass table because it affects the potential energy surface driving two colliding nuclei to the CN. The capture cross section depends on the deformations predicted for the colliding nuclei. So, in the present article, employing the mass table of Ref. [21–23] based on the microscopic-macroscopic method, we will predict the excitation functions in the xn -, pxn -, and αxn -evaporation channels of the ^{48}Ca -induced complete fusion reactions and, correspondingly, the maximum cross sections at the optimal energies of these channels.

II. MODEL

For the excited SHN, the emission of charged particles is suppressed by the high Coulomb barrier and competes with the neutron evaporation and fission. The evaporation residue cross section can be written in factorized form [17, 20, 24–38]:

$$\sigma_s(E_{\text{c.m.}}) = \sum_{J=0} \sigma_{\text{cap}}(E_{\text{c.m.}}, J) P_{\text{CN}}(E_{\text{c.m.}}, J) W_s(E_{\text{c.m.}}, J). \quad (1)$$

The evaporation residue cross section in the evaporation channel s depends on the partial capture cross section σ_{cap} for the transition of the colliding nuclei over the entrance (Coulomb) barrier, the probability of CN formation P_{CN} after the capture and the survival probability W_s of the excited CN. The formation of CN is described within a version of the dinuclear system model [17, 20, 37, 38].

In the first step of fusion reaction the projectile is captured by the target. In the calculation of σ_{cap} in Eq. (1), the orientation of the deformed actinide target nuclei is taken into account [37]. The bombarding energy $E_{\text{c.m.}}$ at which the capture for all orientation becomes possible is defined by the Coulomb barrier at sphere-side orientation. At smaller $E_{\text{c.m.}}$ some partial waves fall under the barrier. The position and height of the Coulomb barrier are mainly affected by the quadrupole deformation of actinide nucleus. The quadrupole deformation used were extracted in Ref. [39] from the measured quadrupole moments. So, the effect of deformations of higher multipolarities is taken partially into consideration in our calculations. Because the uncertainty in quadrupole deformation affects the Coulomb bar-

rier stronger than the hexadecopole deformation, we consider only quadrupole deformation in our calculations.

In the second step the formed dinuclear system (DNS) evolves to the CN in the mass asymmetry coordinate $\eta = (A_1 - A_2)/(A_1 + A_2)$ (A_1 and A_2 are the mass numbers of the DNS nuclei) [17, 20, 24–28, 30–38]. Because the bombarding energy $E_{c.m.}$ of the projectile is usually higher than the Q value for the CN formation, the produced CN is excited.

When successful, hot fusion creates a heavy nucleus in a highly excited state that rapidly emits two, three or four fast neutrons, each removing a few MeV of energy from the system, whereby it cools down. At every stage of this emission the neutrons compete with the fission processes that lead to nucleus splitting. This means that the nucleus generated through hot fusion must be resistant to nuclear fission and explain great importance of the fission barrier B_f as the main parameter which protect nucleus against fission. In another words, in the third step of the reaction the CN loses its excitation energy mainly by the emission of particles and γ -quanta [40–47]. In the de-excitation of CN, the particle emission competes with the fission which is the most probable process besides fission in normal nuclei. In this paper, we describe the production of nuclei in the evaporation channels with emission of charged particle (proton or α -particle) and neutrons as in Refs. [17, 20, 38]. The emissions of γ , deuteron, triton, and clusters heavier than alpha-particle are expected to be negligible to contribute to the total width of the CN decay. The de-excitation of the CN is treated with the statistical model using the level densities from the Fermi-gas model. The neutron separation energies B_n , Q -values for proton and alpha-particle emissions, the nuclear mass excesses of SHN, and the fission barriers for the nuclei considered are taken from the microscopic-macroscopic model [21–23]. Recently, within this approach (with parameters adjusted to heavy nuclei [48]), it was possible to reasonably reproduce data on ground state masses; first, second and third [22, 49–54] fission barriers in actinides nuclei for which some empirical/experimental data are available.

Within the microscopic-macroscopic method, the energy of deformed nucleus is calculated as a sum of two parts: the macroscopic one being a smooth function of Z , N and deformation, and the fluctuating microscopic one that is based on some phenomenological single-particle potential. The deformed Woods-Saxon potential model used here is defined in terms of the nuclear surface. Mononuclear shapes can be parameterized via nuclear radius expansion in spherical harmonics $Y_{lm}(\vartheta, \varphi)$. We admit shapes defined by the following equation of the

TABLE I: The theoretical barriers V_i and energy thresholds $B_i = V_i - Q_i$ in the evaporation channels with emission of proton and alpha-particle ($i = p, \alpha$). The $Q_{p,\alpha}$ -values are calculated with the microscopic-macroscopic models [19] and [21].

Reaction	V_p (MeV)	V_α (MeV)	B_p [21] (MeV)	B_α [21] (MeV)	B_p [19] (MeV)	B_α [19] (MeV)
$^{48}\text{Ca} + ^{242}\text{Pu}$	12.6	25.1	16.7	15.0	17.1	16.6
$^{48}\text{Ca} + ^{244}\text{Pu}$	12.6	25.1	16.1	15.7	17.2	16.9
$^{48}\text{Ca} + ^{243}\text{Am}$	12.7	25.3	14.5	14.1	14.1	15.7
$^{48}\text{Ca} + ^{245}\text{Cm}$	12.8	25.5	15.5	14.7	15.5	14.6
$^{48}\text{Ca} + ^{248}\text{Cm}$	12.7	25.5	16.1	14.6	15.9	14.4
$^{48}\text{Ca} + ^{249}\text{Bk}$	12.8	25.6	14.0	14.1	14.2	13.9
$^{48}\text{Ca} + ^{249}\text{Cf}$	12.9	25.9	15.0	13.6	14.8	13.8
$^{48}\text{Ca} + ^{251}\text{Cf}$	12.9	25.9	15.7	14.0	15.1	13.3

TABLE II: Calculated Q_α -values [21] and experimental $Q_\alpha^{exp.}$ -values [3] for the indicated SHN.

SHN	Q_α (MeV)	$Q_\alpha^{exp.}$ (MeV)	SHN	Q_α (MeV)	$Q_\alpha^{exp.}$ (MeV)
^{294}Og	12.09	11.81	^{288}Fl	10.32	10.07
^{294}Ts	11.25	11.12	^{287}Fl	10.44	10.16
^{293}Ts	11.45	11.36	^{286}Fl	10.80	10.37
^{293}Lv	10.80	10.68	^{286}Nh	9.68	9.89
^{292}Lv	10.92	10.77	^{285}Nh	10.27	10.33
^{291}Lv	10.89	10.89	^{284}Nh	10.34	10.30
^{290}Lv	11.14	10.99	^{282}Nh	10.71	10.78
^{290}Ms	10.11	10.42	^{278}Nh	11.56	11.85
^{289}Ms	10.56	10.69	^{285}Cn	9.35	9.32
^{288}Ms	10.54	10.70	^{283}Cn	9.91	9.67
^{287}Ms	10.61	10.74	^{281}Cn	10.78	10.46
^{289}Fl	9.93	9.97	^{277}Cn	11.66	11.62

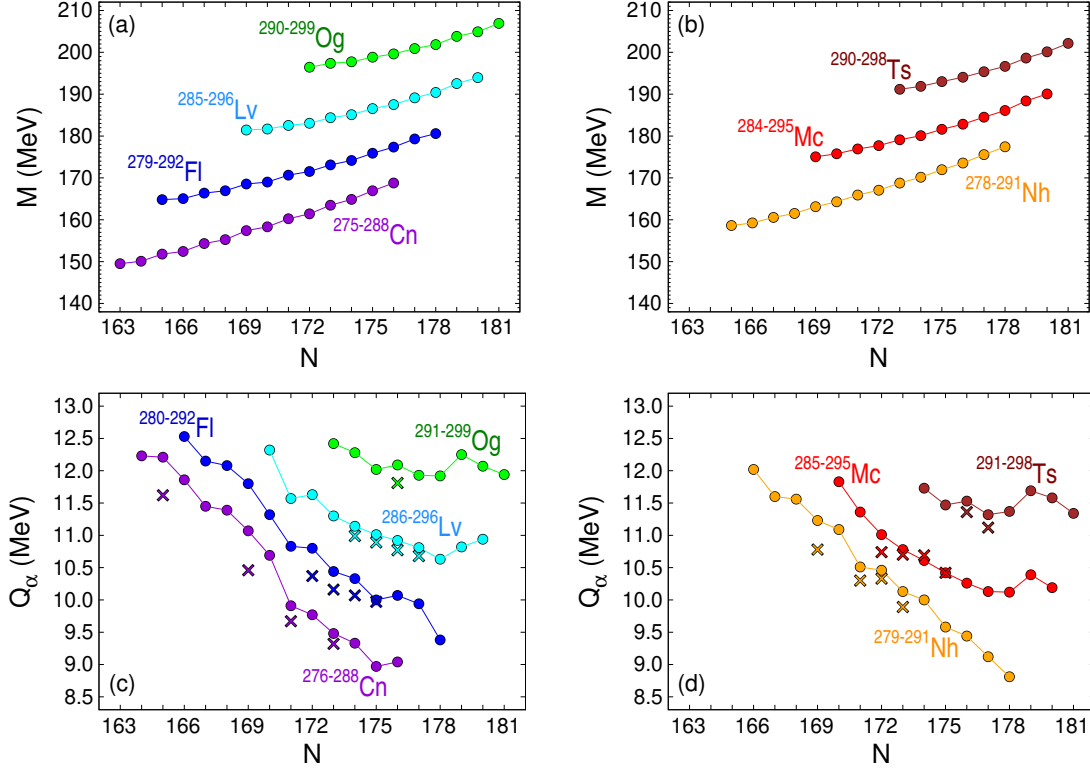


FIG. 1: Nuclear masses: M (top panels) and Q_α -values (bottom panels) for even- Z (left hand-side panels): $^{275-288}\text{Cn}$, $^{279-292}\text{Fl}$, $^{286-296}\text{Lv}$, $^{291-299}\text{Og}$ and odd- Z (right hand-side panels): $^{279-291}\text{Nh}$, $^{285-295}\text{Mc}$, $^{291-298}\text{Ts}$. Experimental data for Q_α are taken from [3].

nuclear surface:

$$R(\vartheta, \varphi) = c(\{\beta\})R_0\left\{1 + \sum_{\lambda=1}^{\infty} \sum_{\mu=-\lambda}^{+\lambda} \beta_{\lambda\mu} Y_{\lambda\mu}(\vartheta, \varphi)\right\}, \quad (2)$$

where $c(\{\beta\})$ is the volume-fixing factor and R_0 is the radius of a spherical nucleus.

The $n_p = 450$ lowest proton levels and $n_n = 550$ lowest neutron levels from $N_{max} = 19$ lowest shell of the deformed oscillator are taken into account in the diagonalization procedure. We have determined the single-particle spectra for every investigated nucleus. The Strutinsky smoothing was performed with the 6-th order polynomial and the smoothing parameter equal to $1.2\hbar\omega_0$. For the systems with odd proton or neutron (or both), we use the standard blocking method. Considered configurations consist of an odd particle occupying one of the levels close to the Fermi level and the rest of particles forming paired BCS state on remaining levels. The ground states were found by minimizing over configurations (blocking particles on levels from the 10-th below to 10-th above the Fermi level) and deformations.

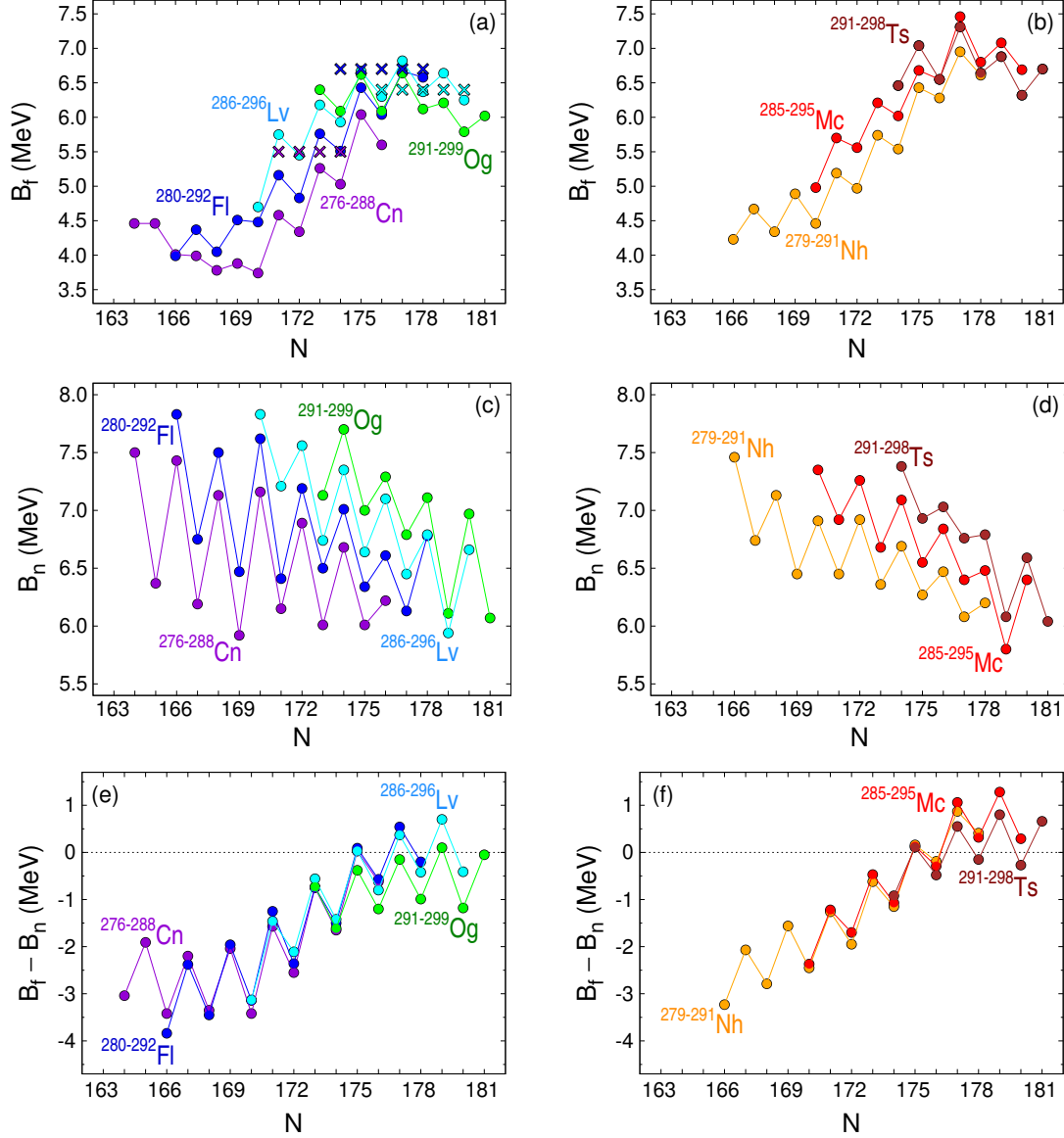


FIG. 2: Fission barriers: B_f (top panels), neutron separation energies: B_n (middle panels) and their differences: $B_f - B_n$ (bottom panels) for even- Z (left-hand side panels): $^{275-288}\text{Cn}$; $^{279-292}\text{Fl}$; $^{286-296}\text{Lv}$; $^{291-299}\text{Og}$ and odd- Z (right-hand side panels): $^{279-291}\text{Nh}$; $^{285-295}\text{Mc}$; $^{291-298}\text{Ts}$. Experimental data for barriers, marked by crosses, are taken from [72].

For nuclear ground states it was possible to confine analysis to axially-symmetric shapes. More details can be found in Ref. [22]. The simplest extension of the WS model to odd nuclei required three new constants which may be interpreted as the mean pairing energies for even-odd, odd-even and odd-odd nuclei [22]. They were fixed by a fit to the masses with $Z \geq 82$ and $N > 126$ via minimizing the rms deviation in particular groups of nuclei what

is rather standard procedure [55, 56]. The experimental nuclear masses of heavy nuclei were taken from [57]. The obtained rms deviation in masses for 252 nuclei is about 400 keV with blocking scenario [22] used here. Similar rms error is obtained for 204 Q_α values. For 88 measured Q_α values in SHN, the quantities outside the region of the fit, we obtained the rms deviation of about 250 keV [22].

To estimate the survival probability, the fission barriers from adiabatic scenario, i.e. the smallest possible ones, are taken [23]. The main problem in a search for saddle points is that, since they are neither minima nor maxima, one has to know energy on a multidimensional grid of deformations (the often used and much simpler method of minimization with imposed constraints may produce invalid results) [50, 58–60]. To find saddles on a grid we used the Imaginary Water Flow technique. This conceptually simple and at the same time very efficient (from a numerical point of view) method was widely used and discussed [50, 58, 61–64]. Based on this and our previous results showing that triaxial saddles are abundant in SHN [54], we consider that quadrupole triaxial shapes have to be included for the first barriers with which we are dealing with the nuclei considered here. So, the saddle points are searched in the five dimensional deformation space spanned by: β_{20} , β_{22} , β_{40} , β_{60} , β_{80} - defined in Eq. (2), using the Imaginary Water Flow technique. All details regarding the methodology of searching for the right saddles with the exact specification of the deformation spaces used, can be found in Ref. [23]. Finally, we want to emphasize, that recently we have systematically determined inner and outer fission barrier heights for 75 actinides, within the range from actinium to californium, including odd- A and odd-odd systems, for which experimental estimates were accessible [53]. A statistical comparison of our inner and outer fission barrier heights with available experimental estimates gives the average discrepancy and the rms deviation not larger than 0.82 MeV and 0.94 MeV, respectively. This allows us to have some confidence in the macroscopic-microscopic model used here. Significant differences in the fission barriers obtained in various modern nuclear models were noticed in Ref. [65]. A broad discussion of the problems arising from this can be found in Refs. [23, 66].

Owing to the dependence of the shell effects on nuclear excitation, the value of shell correction effectively depends on the excitation energy with the damping parameter $E_d = 25$ MeV. In comparison to Refs. [18, 67, 68], which are based for even-even nuclei on the same mass table, we employ the equivalent method to calculate the survival probability [17, 20, 38] taking into account the shell effect damping in the potential energy surface and

asymptotic level-density parameter a . However, we would like to emphasise that for odd nuclei in Refs. [18, 67, 68] the pairing was treated in different way compared to nuclear input data used here. Namely, the predictions of the Fusion-by-Diffusion model [18, 67, 68] for the synthesis cross sections of 114120 elements were based on the macroscopic-microscopic properties calculated within the quasiparticle method in pairing channel. The ground states and consequently fission barrier heights for other nuclei were calculated separately by adding the energy of the odd particle occupying a single-particle state. This quasiparticle energy E_{qp} in the superconducting state takes a simple form: $E_{qp} = \sqrt{(\varepsilon_{qp} - \lambda)^2 + \Delta^2}$, where ε_{qp} is the energy of the odd nucleon in the quasiparticle state, λ is the Fermi energy and Δ is the pairing gap energy. In this scenario of fission barriers calculation the energy E_{qp} was added at every grid point as well as at every minimisation step in the gradient procedure used for the ground states. So, the calculations of masses and B_f have been performed without blocking of any state in the calculations within the Fusion-by-Diffusion model [18, 67, 68] but with using the BSC-quasiparticle method.

In the DNS model used here the damping parameter should be larger than in Refs. [18, 67, 68]. With the expression $a_n = a = A/10 \text{ MeV}^{-1}$ for the asymptotic level-density parameter for neutron (A is the mass number of the CN) we obtain almost the same values as those used in Ref. [69] and found microscopically in Ref. [70]. The level-density parameters for fission, proton-emission, and α -emission channels are taken as $a_f = 0.98a$, $a_p = 0.96a$, and $a_\alpha = 1.15a$, respectively. The ratio between a and a_f is closed to that found in Ref. [70]. Here, we set these parameters for all reactions considered. Because the shell corrections at the ground state are larger with the mass table [19], in Refs. [17, 20] the larger values of $a_f = 1.03a$ were used. Other parameters in Refs. [17, 20] were set the same as in this paper. So, taking other mass table for the properties of SHN, we change only the ratio a_f/a .

For the calculation of the Coulomb barrier, we use the expression

$$V_j = \frac{(Z - z_j)z_j e^2}{r_j[(A - m_j)^{1/3} + m_j^{1/3}]}, \quad (3)$$

where z_j (m_j) are the charge (mass) numbers of the charged particle (proton or α -particle) and r_j is a constant. The charge Z (mass A) number corresponds to the CN. There are different theoretical estimations of r_j [40, 47]. In the case of α -emission, r_α varies from 1.3 to 1.78 fm. We obtain r_α from the energy of the DNS formed by the daughter nucleus and α -particle. We calculate the Coulomb barrier in the interaction potential between the

α -particle and the daughter nucleus [71], and find the value of r_α from Eq. (3). For different nuclei considered, we obtained $r_\alpha = 1.57$ fm using this method. Thus, in the calculations of V_α we set $r_\alpha = 1.57$ fm for nuclei considered. The parameter r_p for the Coulomb barrier for proton emission is taken as $r_p=1.7$ fm from Refs. [35, 47]. With these values of r_α and r_p Eq. (3) results in V_α and V_p which are about 2.5 and 1.5 MeV (Table II), respectively, larger than those used in Refs. [18, 67, 68]. As shown in Refs. [18, 67, 68], the increase of V_α and V_p by 4 MeV leads to about one order of magnitude smaller σ_s in the αxn and pxn evaporation channels. So, the difference of our r_α and r_p from those in Refs. [18, 67, 68] could create 2–4 times difference in the values of σ_s . In Refs. [17, 20], the same values of V_α and V_p were used as in this paper. As seen in Table II, the values of energy thresholds for protons and alpha-particles obtained with the mass table [19] deviate within 2.5 MeV from those calculated with the mass table [21].

As found, the values of σ_s near the maxima of excitation functions are almost insensitive to the reasonable variations of the parameters used, but far from the maxima they change up to one order of magnitude. Therefore, the results obtained in this paper have quite a small uncertainty near the maxima of excitation functions which are important to get the maximum yield of certain nucleus in the experiments. We estimate the uncertainty of our calculations of σ_s within a factor of 2–4. Our model was well tested in Ref. [38] for many reactions in which the excitation functions of transfermium nuclei produced in the charged particle evaporation channels have been measured.

III. CALCULATED RESULTS

In Fig. 1, our results for nuclear masses (top panels) and calculated from them Q_α -values (bottom panels) for SHN considered in this article are shown. As one can see, the available alpha-decay energy measurements are perfectly reproduced. Only in the case of Cn and Nh nuclei with smaller number of neutrons our results slightly overestimate the experimental data. The exact values in some of the most important cases here are summarized in the Table II. Let us emphasize that only ground-state-to-ground-state alpha transition were calculated. Apparent Q_α values taking the parent ground-state configuration in odd and odd-odd systems as the final state in daughter were not considered. This may be the reason for the overestimation in a few cases, as especially in odd nuclei the decay may occur to

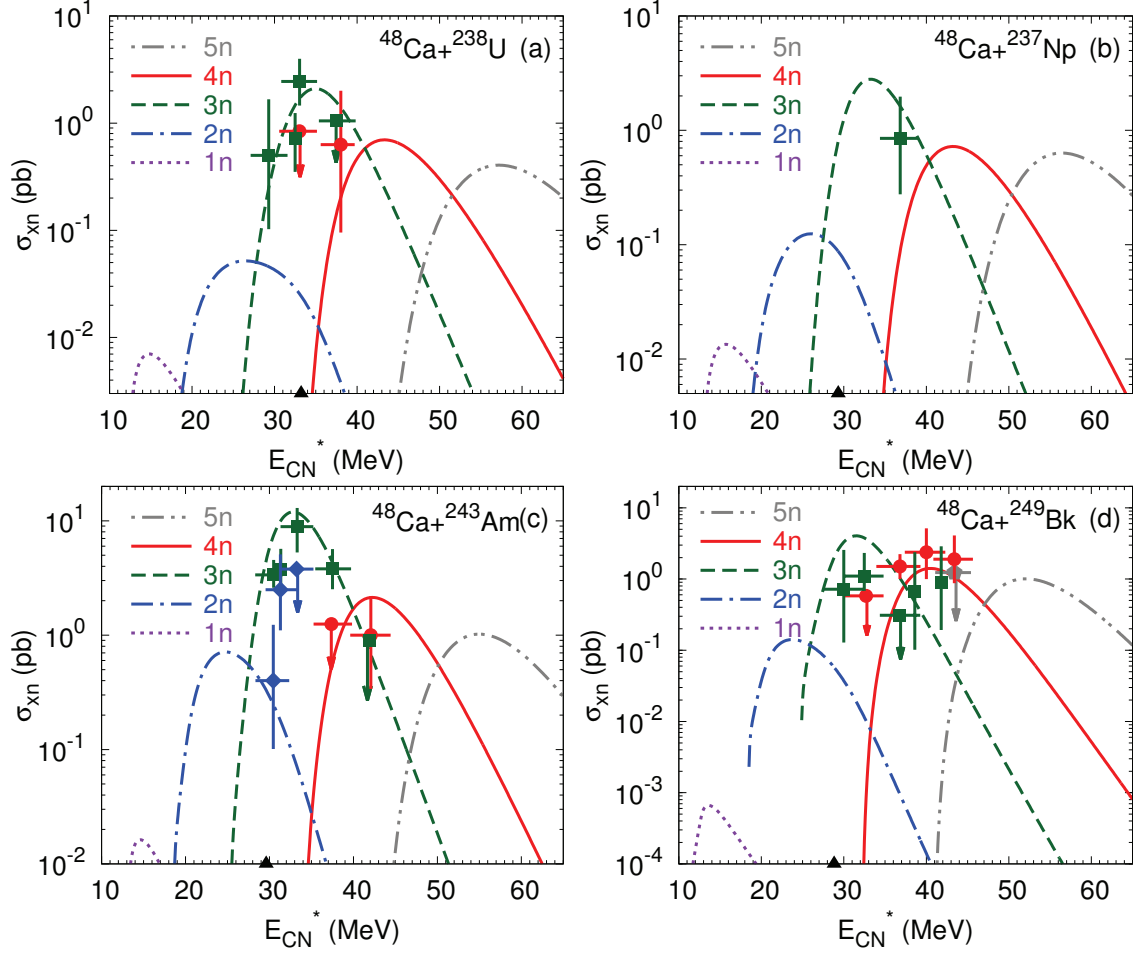


FIG. 3: The measured (symbols) and calculated (lines) excitation functions for xn -evaporation channels ($x = 1 - 5$) of the indicated complete fusion reactions. The mass table of Ref. [21] is used in the calculations. The black triangles at energy axis indicate the excitation energy E_{CN}^* of the CN at bombarding energy corresponding to the Coulomb barrier for the sphere-side orientation. The blue diamonds, green squares, red circles, and gray pentagons represent the experimental data [3] with error bars for $2n$ -, $3n$ -, $4n$ -, and $5n$ -evaporation channels, respectively. The vertical lines with arrow indicate the upper limits of evaporation residue cross sections.

excited states of the daughter nucleus, which shortens the alpha transition lines.

In Fig. 2 we provide a comparison of our calculated fission barriers with the available experimental estimates based on the observed evaporation residue production probabilities [72]. As in the case of Fig. 1, the isotopes: Fl, Cn, Lv and Og are shown on the left-hand side while Nh, Mc, Ts on the right-hand side. As seen in Fig. 2, our calculated fission barriers B_f are in quite good agreement with the experimental (empirical) estimates [72] marked

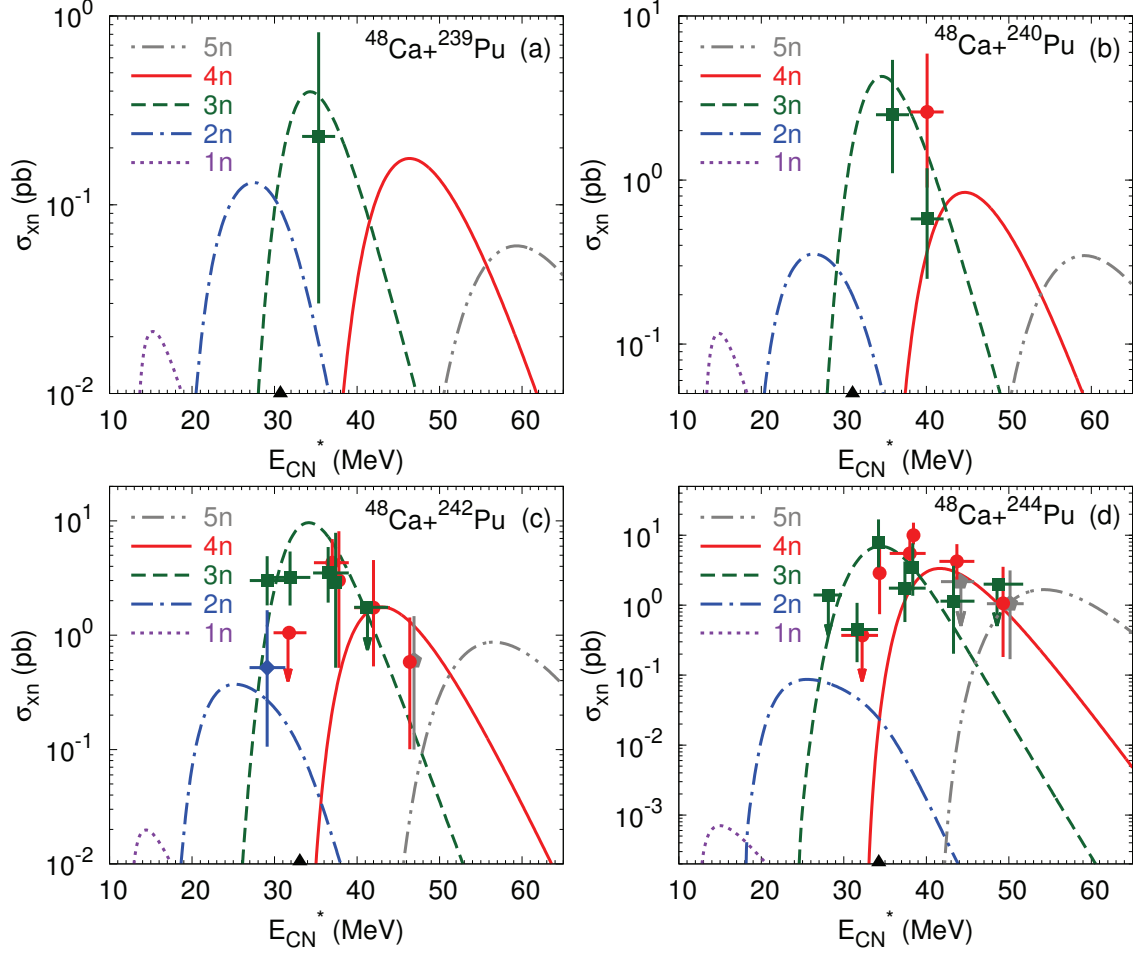


FIG. 4: The same as in Fig. 3, but for other indicated complete fusion reactions.

by crosses. For completeness, we show the neutron separation energies B_n in the middle part of Fig. 2. The strong staggering is clearly visible. As mentioned before, the height of this threshold in relation to the fission barrier is crucial for determining which process wins the competition in nuclear decay, fission or neutron emission. In Fig. 2 (bottom panels), the differences between these two key parameters controlling survival probability are also shown.

With the nuclear properties from Refs. [21–23] the calculated excitation functions for xn evaporation channels are presented in Figs. 3–5 for the complete fusion reactions $^{48}\text{Ca} + ^{238}\text{U}$, ^{237}Np , ^{243}Am , ^{249}Bk , $^{239,240,242,244}\text{Pu}$, $^{245,248}\text{Cm}$, $^{249,251}\text{Cf}$. In Ref. [20] and here, the same model is used to calculate the evaporation residue cross sections. So, the comparison with the results of Ref. [20] reflects the difference in the predicted properties of SHN. In comparison to Ref. [20] the bombarding energies corresponding to the Coulomb barriers

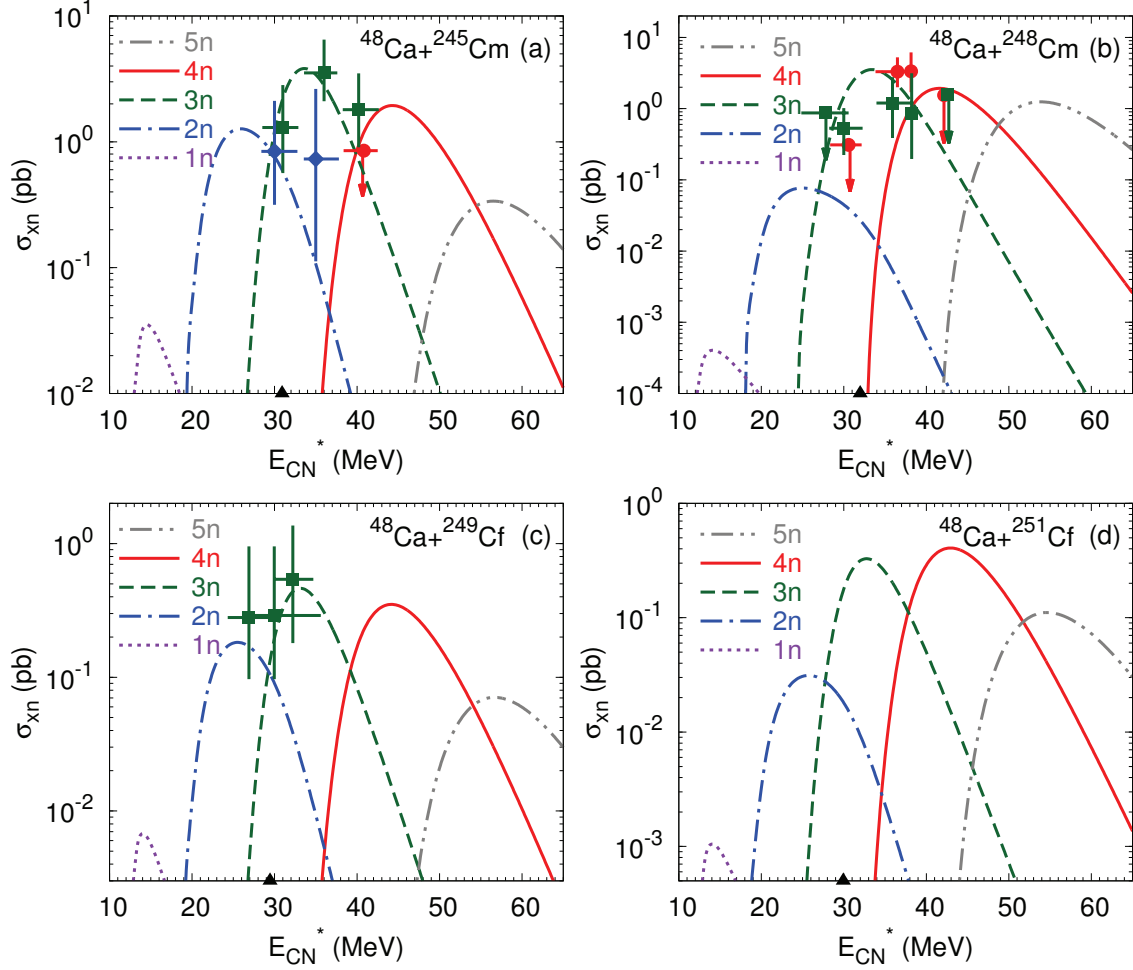


FIG. 5: The same as in Fig. 3, but for other indicated complete fusion reactions.

for the sphere-side orientations lead to 2–3 MeV smaller E_{CN} . As a result, the maxima of excitation functions $\sigma_{xn}(E_{CN})$ are slightly shifted to higher E_{CN} in Figs. 3-5. If in Ref. [20] $\sigma_{4n} > \sigma_{3n}$ in the maxima of excitation functions for the reactions $^{48}\text{Ca}+^{242,244}\text{Pu}, ^{245,248}\text{Cm}$, the present calculations with the data of Ref. [21] result in $\sigma_{4n} < \sigma_{3n}$ and larger σ_{3n}/σ_{2n} . Though in the reactions $^{48}\text{Ca}+^{238}\text{U}, ^{237}\text{Np}, ^{243}\text{Am}, ^{249}\text{Bk}$ the maximum production cross sections are expected in the 3n evaporation channel independently on the mass table, in Fig. 3 the ratios σ_{3n}/σ_{4n} are about 2 times smaller than those in Ref. [20]. The mass table [21] leads to close maxima of σ_{3n} and σ_{4n} , relatively large σ_{5n} and smaller σ_{2n} in most reactions.

The maximum cross sections in the 2n-evaporation channel were found to be within factor of 10 smaller than the cross sections at the maxima of excitation functions of the 3n– or 4n–evaporation channels. The cross sections in 1n evaporation channel could be of interest for the experimental study if they are larger than 5 fb. Thus, employing reactions in the

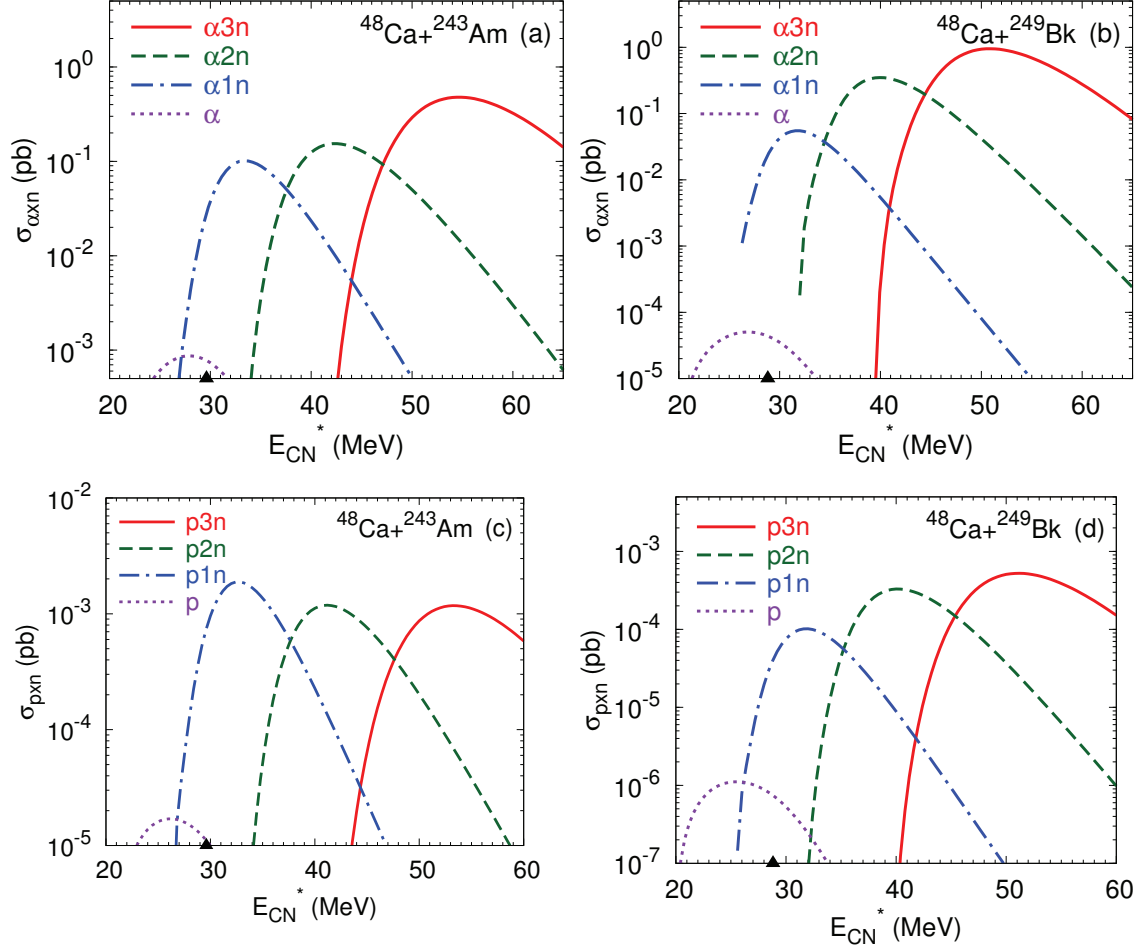


FIG. 6: The same as in Fig. 3, but for αxn -evaporation channels ($x = 0 - 3$) of the indicated complete fusion reactions.

$1n$ - and $2n$ -evaporation channels, one can directly produce heaviest isotopes closer to the center of "the island of stability": $^{284,285}\text{Cn}$, $^{283,284}\text{Nh}$, ^{294}Lv , ^{295}Ts , and $^{295-297}\text{Og}$. Many of them were only produced as daughters in the α -decay chains. The isotopes ^{295}Ts , and $^{295-297}\text{Og}$ are presently unknown.

The comparison of the results in Figs. 3-5 with those in Refs. [67, 68] based on the same mass table allows us to stress the difference of the fusion models used. In spite of the difference of the fusion models, the predicted values of cross sections are rather close for most reactions. While $\sigma_{4n} > \sigma_{3n}$ for the $^{48}\text{Ca} + ^{249}\text{Cf}$ reaction in Ref. [67], in Fig. 5 we obtain $\sigma_{4n} < \sigma_{3n}$. For the $^{48}\text{Ca} + ^{249}\text{Bk}$, we obtain smaller ratio σ_{4n}/σ_{5n} and larger σ_{3n}/σ_{4n} than those in Ref. [68].

The calculated excitation functions for the channels with evaporation of charged particle

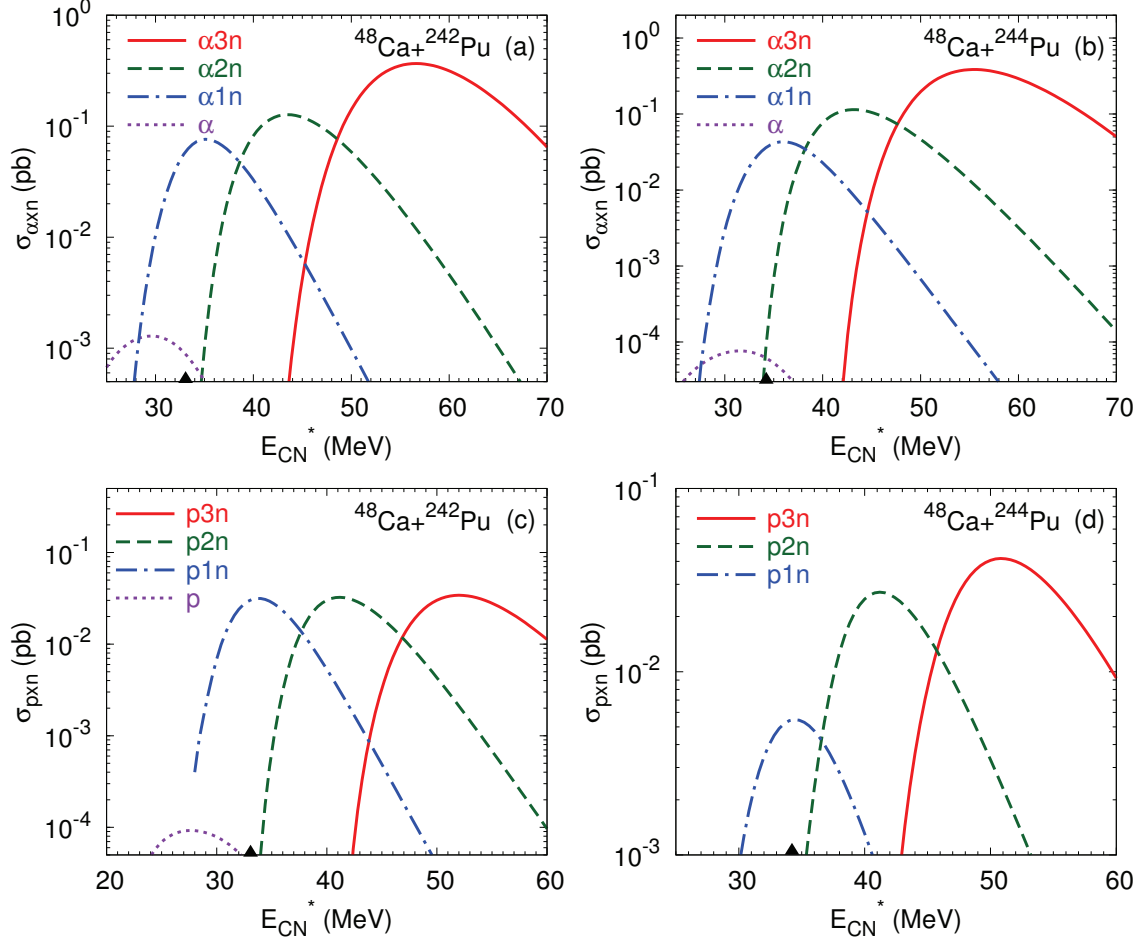


FIG. 7: The same as in Fig. 3, but for αxn - and $p xn$ -evaporation channels ($x = 0 - 3$) of the indicated complete fusion reactions.

are presented in Figs. 6-9. While in Ref. [17] $\sigma_{\alpha 2n} > \sigma_{\alpha 3n}$ and $\sigma_{p 2n} > \sigma_{p 3n}$ with mass table [19] in most reactions, we obtain rather close cross sections in $\alpha 2n$ and $\alpha 3n$, $p 2n$ and $p 3n$ evaporation channels due to slightly smaller neutron separation energies in the mass table [21–23]. Because the same mass table is used (with a reservation regarding the different treatment of odd particles) in Ref. [18], the predicted cross sections are similar there to those in Figs. 6-9. However, stronger dependence of fusion probability P_{CN} on energy leads to relative increase of the $\alpha 3n$ and $p 3n$ evaporation channels in Figs. 6-9. The relatively smaller yields in the $\alpha 1n$ and $p 1n$ evaporation channels are due to the same reason.

The production cross sections of almost all of these SHN in the xn -evaporation channels are comparable or even larger than those in the charged particle evaporation channels. The production cross sections of heaviest isotopes $^{287-290}\text{Nh}$, $^{291-293}\text{Mc}$, and $^{295-296}\text{Ts}$ ($^{286,287}\text{Cn}$,

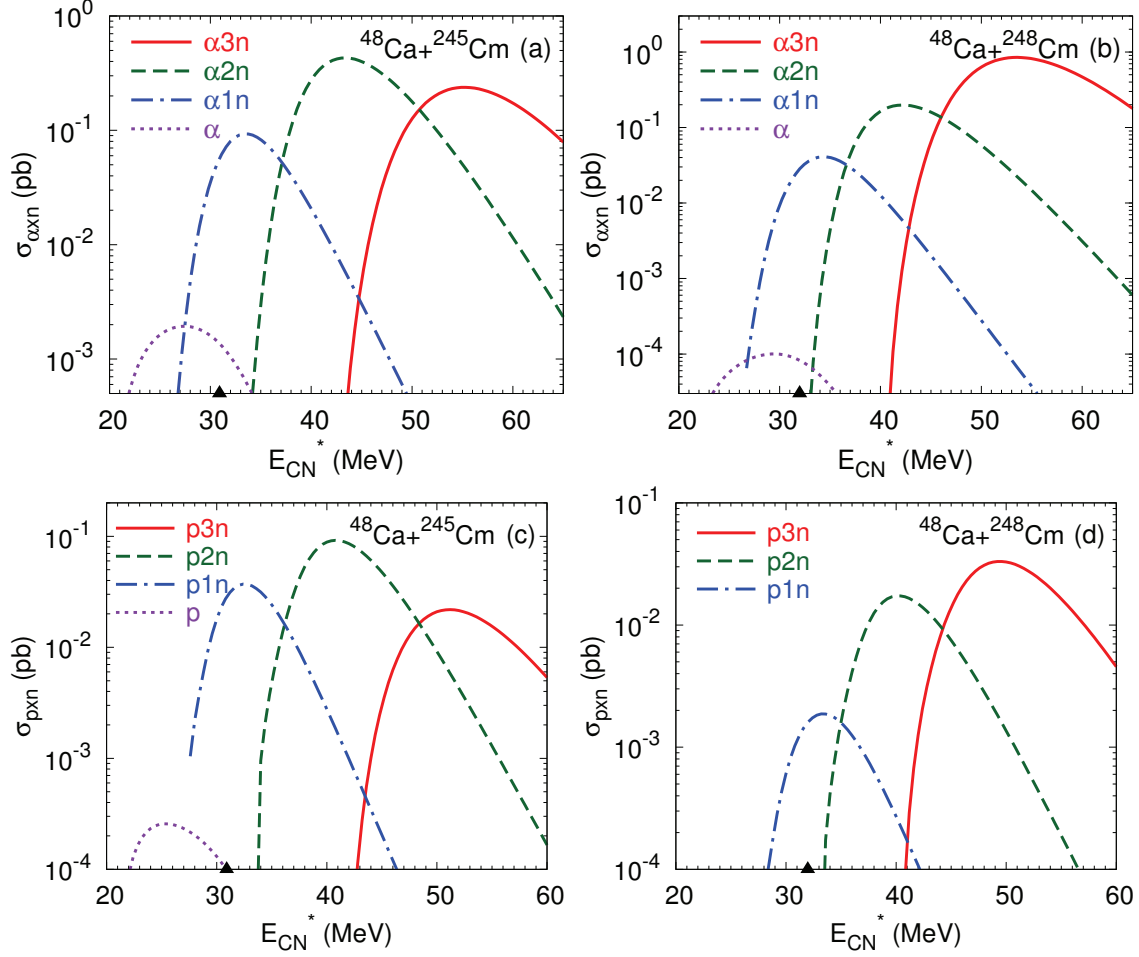


FIG. 8: The same as in Fig. 3, but for αxn - and $p xn$ -evaporation channels ($x = 0 - 3$) of the indicated complete fusion reactions.

^{286}Nh , $^{290,291}\text{Fl}$, $^{291,292}\text{Mc}$, and ^{294}Lv) in the $p xn$ -channels (αxn -channels) of the ^{48}Ca -induced fusion reactions were predicted: about 10–200 fb in the $p xn$ -evaporation channels (about 50–500 fb in the αxn -evaporation channels).

IV. SUMMARY

For the ^{48}Ca -induced actinide-based complete fusion reactions, the excitation functions for the production of the SHN with charge numbers 112–118 were calculated in xn -, αxn -, and $p xn$ -evaporation channels using the predictions of SHN properties from Ref. [21–23].

As it turns out, in modeling of reactions leading to the SHN, the use of a consistent i.e., coming from one source, set of nuclear data input plays a fairly important role. In

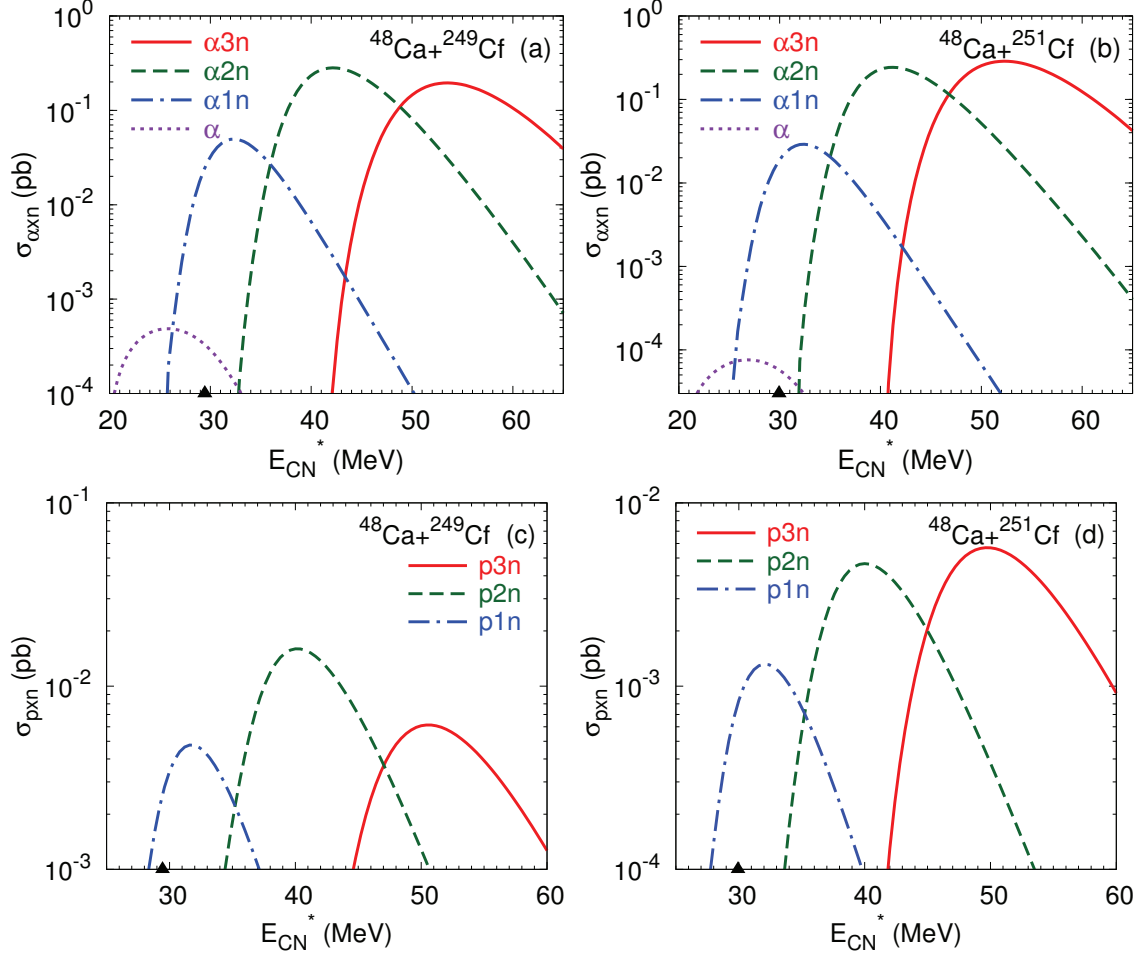


FIG. 9: The same as in Fig. 3, but for αxn - and $p xn$ -evaporation channels ($x = 0 - 3$) of the indicated complete fusion reactions.

the presented article, all used nuclear properties of the ground states and saddle points were calculated within the multidimensional macroscopic-microscopic approach with blocking technique for odd nuclei.

Obtained agreement of cross-sections for the reactions in $3n$ channel is excellent. Excitation functions are only slightly shifted towards higher energies compared to the experiment when four neutrons are emitted in the cascade. Only for the reactions; $^{48}\text{Ca} + ^{240}\text{Pu}$ and $^{48}\text{Ca} + ^{242}\text{Pu}$, the resulting cross-sections are underestimated - but less than one order of magnitude.

The use of the charged particle evaporation channels allows us to increase the mass number of heaviest isotopes of nuclei with $Z = 113, 115$, and 117 (112 and 114) up to $5, 3$, and 1 (1 and 1) units, respectively, with respect to the xn evaporation channels. In addition,

in the nuclei produced the electron capture can occur by adding one more neutron in the daughter nuclei. The proton evaporation channels seem to be more effective to approach $N = 184$ than the alpha emission channels. One can produce more neutron-rich isotopes in the reactions with even- Z targets than in the reactions with odd- Z ones. The pxn - and αxn -evaporation channels allows us to obtain an access to those isotopes which are unreachable in the xn -evaporation channels due to the lack of proper projectile-target combination. Thus, employing reactions suggested, one can produce the heaviest isotopes closer to the center of the island of stability. The pxn - and αxn -evaporation channels can be only distinguished by different α -decay chains of the evaporation residues because the excitation functions of these channels overlap with those from xn -evaporation channels.

Our present results were compared with those obtained with the same fusion model and other mass table and with completely other fusion model [18, 67, 68] for which nuclear properties were calculated using the same macroscopic-microscopic model but with quasiparticle method for pairing. Absolute values of cross sections are rather close. However, the ratio of the cross sections in the maxima of excitation functions is sensitive to the mass table. For example, $\sigma_{p2n} > \sigma_{p3n}$ with the mass table [19], while $\sigma_{p2n} \approx \sigma_{p3n}$ in the calculations presented. If the same mass table is used with different fusion model, the fusion probability creates the difference in the cross sections obtained. For example, the ratios σ_{5n}/σ_{4n} and $\sigma_{\alpha 2n}/\sigma_{\alpha 3n}$ are sensitive to the increase rate of P_{CN} with excitation energy and, thus, to the fusion model.

Acknowledgments

G.G.A. and N.V.A. acknowledge the partial supports from the Alexander von Humboldt-Stiftung (Bonn). This work was partly supported by RFBR (17-52-12015, 20-02-00176), DFG (Le439/6-1), and Tomsk Polytechnic University Competitiveness Enhancement Program grant. M.K. was co-financed by the National Science Centre under Contract No. UMO-2013/08/M/ST2/00257 (LEA-COPIGAL).

[1] Yu.Ts. Oganessian, J. Phys. G **34**, R165 (2007).

- [2] Yu.Ts. Oganessian *et al.*, Phys. Rev. Lett. **104**, 142502 (2010); Phys. Rev. C **87**, 014302 (2013); Phys. Rev. C **87**, 034605 (2013); Phys. Rev. C **87**, 054621 (2013); V.K. Utyonkov *et al.*, Phys. Rev. C **92**, 034609 (2015).
- [3] Yu.Ts. Oganessian and V.K. Utyonkov, Nucl. Phys. A **944**, 62 (2015).
- [4] R. Eichler *et al.*, Nature **447**, 72 (2007).
- [5] S. Hofmann *et al.*, Eur. Phys. J. A **32**, 251 (2007).
- [6] L. Stavsetra, K.E. Gregorich, J. Dvorak, P.A. Ellison, I. Dragojevic, M.A. Garcia, and H. Nitsche, Phys. Rev. Lett. **103**, 132502 (2009).
- [7] Ch. Düllmann *et al.*, Phys. Rev. Lett. **104**, 252701 (2010).
- [8] J.M. Gates *et al.*, Phys. Rev. C **83**, 054618 (2011).
- [9] S. Hofmann *et al.*, Eur. Phys. J. A **48**, 62 (2012).
- [10] J.M. Khuyagbaatar *et al.*, Phys. Rev. Lett. **112**, 172501 (2014).
- [11] S. Hofmann *et al.*, Eur. Phys. J. A **52**, 180 (2016).
- [12] A. Sobiczewski, F.A. Gareev, and B.N. Kalinkin, Phys. Lett. B **2**, 500 (1966); H. Meldner, Ark. Fys. **36**, 593 (1967); S.G. Nilsson, J.R. Nix, A. Sobiczewski, Z. Szymanski, S. Wycech, C. Gustafson, and P. Möller, Nucl. Phys. **A115**, 545 (1968); U. Mosel and W. Greiner, Z. Phys. **222**, 261 (1969); E.O. Fiset and J. R. Nix, Nucl. Phys. **A193**, 647 (1972). J. Randrup, S.E. Larsson, P. Möller, S.G. Nilsson, K. Pomorski, and A. Sobiczewski, Phys. Rev. C **13**, 229 (1976); P. Möller and J. R. Nix, J. Phys. G **20**, 1681 (1994); A. Sobiczewski, Phys. Part. Nuclei **25**, 295 (1994); R. Smolanczuk, J. Skalski, and A. Sobiczewski, Phys. Rev. C **52**, 1871 (1995).
- [13] I. Muntian, Z. Patyk, and A. Sobiczewski, Acta Phys. Pol. B **32**, 691 (2001); I. Muntian, S. Hofmann, Z. Patyk, and A. Sobiczewski, Acta Phys. Pol. B **34**, 2073 (2003); O. Parkhomenko, I. Muntian, Z. Patyk, and A. Sobiczewski, Acta Phys. Pol. B **34**, 2153 (2003); I. Muntian, Z. Patyk, and A. Sobiczewski, Phys. Atom. Nucl. **66**, 1015 (2003).
- [14] S. Cwiok, J. Dobaczewski, P.H. Heenen, P. Magierski, and W. Nazarewicz, Nucl. Phys. **A611**, 211 (1996). K. Rutz, M. Bender, T. Bürvenich, T. Schilling, P.G. Reinhard, J.A. Maruhn, and W. Greiner, Phys. Rev. C **56**, 238 (1997); A.T. Kruppa, M. Bender, W. Nazarewicz, P.-G. Reinhard, T. Vertse, and S. Cwiok, Phys. Rev. C **61**, 034313 (2000); M. Bender, P.H. Heenen, and P.G. Reinhard, Rev. Mod. Phys. **75**, 121 (2003); J. Meng, H. Toki, S.G. Zhou, S.Q. Zhang, W.H. Long, and L.S. Geng, Prog. Part. Nucl. Phys. **57**, 470 (2006).

- [15] S. Hofmann and G. Münzenberg, *Rev. Mod. Phys.* **72**, 733 (2000).
- [16] Yu.Ts. Oganessian, *Private communications* (2015 and 2016).
- [17] J. Hong, G.G. Adamian, and N.V. Antonenko, *Phys. Lett. B* **764**, 42 (2017).
- [18] K. Siwek-Wilczyńska, T. Cap, and M. Kowal, *Phys. Rev. C* **99**, 054603 (2019).
- [19] P. Möller, J.R. Nix, W.D. Myers, and W.J. Swiatecki, *At. Data. Nucl. Data. Tables.* **59**, 185 (1995).
- [20] J. Hong, G.G. Adamian, and N.V. Antonenko, *Phys. Lett. B* **805**, 135438 (2020).
- [21] M. Kowal, P. Jachimowicz, and J. Skalski, arXiv: 1203.5013; P. Jachimowicz, M. Kowal, and J. Skalski (unpublished).
- [22] P. Jachimowicz, M. Kowal, J. Skalski *Phys. Rev. C*, **89**, 024304 (2014).
- [23] P. Jachimowicz, M. Kowal, J. Skalski *Phys. Rev. C*, **95**, 014303 (2017).
- [24] V.V. Volkov, *Izv. Akad. Nauk SSSR, Ser. Fiz.* **50**, 1879 (1986); N.V. Antonenko, E.A. Cherepanov, A.K. Nasirov, V.B. Permjakov, and V.V. Volkov, *Phys. Lett. B* **319**, 425 (1993); *Phys. Rev. C* **51** (1995) 2635.
- [25] G.G. Adamian, N.V. Antonenko, S.P. Ivanova, and W. Scheid, *Nucl. Phys. A* **646** (1999) 29.
- [26] G.G. Adamian, N.V. Antonenko, W. Scheid, and V.V. Volkov, *Nucl. Phys. A* **633**, 409 (1998); *Nuovo Cimento A* **110**, 1143 (1997).
- [27] G.G. Adamian, N.V. Antonenko, and W. Scheid, *Nucl. Phys. A* **678**, 24 (2000).
- [28] G.G.Giardina, S.Hofmann, A.I.Muminov, and A.K.Nasirov, *Eur. Phys. J. A* **8**, 205 (2000); G.G.Giardina, F.Hanappe, A.I.Muminov, A.K.Nasirov, and L.Stuttgé, *Nucl. Phys. A* **671**, 165 (2000); A.K.Nasirov *et al.*, *Nucl. Phys. A* **671**, 342 (2005); H.Q.Zhang *et al.*, *Phys. Rev. C* **81**, 034611 (2010); A.K.Nasirov, G.Mandaglio, G.G.Giardina, A.Sobiczewski, and A.I.Muminov, *Phys. Rev. C* **84**, 044612 (2011).
- [29] W. J. Świątecki, K. Siwek-Wilczyńska, and J. Wilczyński, *Acta Phys. Pol. B* **34**, 2049 (2003); *Phys. Rev. C* **71**, 014602 (2005).
- [30] Z.H.Liu and J.D.Bao, *Phys. Rev. C* **74**, 057602 (2006).
- [31] N.Wang, J.Tian, and W.Scheid, *Phys. Rev. C* **84**, 061601(R) (2011).
- [32] N.Wang, E.G.Zhao, W.Scheid, and S.G.Zhou, *Phys. Rev. C* **85**, 041601(R) (2012); N.Wang, E.G.Zhao, and W.Scheid, *Phys. Rev. C* **89**, 037601 (2014).
- [33] L.Zhu, Z.Q.Feng, C.Li, and F.S.Zhang, *Phys. Rev. C* **90**, 014612 (2014); Z.Q.Feng, G.M.Jin, J.Q.Li, and W.Scheid, *Phys. Rev. C* **76**, 044606 (2007).

- [34] A.S. Zubov, G.G. Adamian, N.V. Antonenko, S.P. Ivanova, and W. Scheid, Phys. Rev. C **68**, 014616 (2003).
- [35] G.G. Adamian, N.V. Antonenko, W. Scheid, and A.S. Zubov, Phys. Rev. C **78**, 044605 (2008).
- [36] G.G. Adamian, N.V. Antonenko, and W. Scheid, *Clustering effects within the dinuclear model*, Lecture Notes in Physics, edited by Christian Beck, **848**, 165 (2012).
- [37] J. Hong, G.G. Adamian, and N.V. Antonenko, Phys. Rev. C **92**, 014617 (2015).
- [38] J. Hong, G.G. Adamian, and N.V. Antonenko, Phys. Rev. C **94**, 044606 (2016); Eur. Phys. J. A **52**, 305 (2016).
- [39] S. Raman, C.W. Nestor, and P. Tikkanen, At. Data Nucl. Data Tables **78**, 1 (2001).
- [40] V.S. Barashenkov and V.D. Toneev, *High Energy Interaction of Particles and Nuclei with Atomic Nuclei* (Atomizdat, Moscow, 1972).
- [41] R. Vandenbosch and J.R. Huizenga, *Nuclear Fission* (Academic Press, New York, 1973).
- [42] A. Ignatyuk, *Statistical Properties of Excited Atomic Nuclei* (Energoatomizdat, Moscow, 1983).
- [43] E.A. Cherepanov, A.S. Iljinov, and M.V. Mebel, J. Phys. G. **9**, 931 (1983).
- [44] K.H. Schmidt and W. Morawek, Rep. Prog. Phys. **54**, 949 (1991).
- [45] A.S. Iljinov *et al.*, Nucl. Phys. A **543**, 517 (1992).
- [46] A.S. Zubov, G.G. Adamian, N.V. Antonenko, S.P. Ivanova, and W. Scheid, Phys. Rev. C **65**, 024308 (2002).
- [47] S.G. Mashnik, A.J. Sierk, and K.K. Gudima, *nucl-th/0208048* (2010).
- [48] I. Muntian, Z. Patyk and A. Sobiczewski, Acta Phys. Pol. B **32**, 691 (2001).
- [49] M. Kowal and J. Skalski, Phys. Rev. C **82**, 054303 (2010).
- [50] P. Jachimowicz, M. Kowal, and J. Skalski, Phys. Rev. C **85**, 034305 (2012).
- [51] M. Kowal and J. Skalski, Phys. Rev. C **85**, 061302(R) (2012).
- [52] P. Jachimowicz, M. Kowal, and J. Skalski, Phys. Rev. C **87**, 044308 (2013)
- [53] P. Jachimowicz, M. Kowal, and J. Skalski Phys. Rev. C, **101**, 014311 (2020).
- [54] M. Kowal, P. Jachimowicz, and A. Sobiczewski, Phys. Rev. C **82**, 014303 (2010).
- [55] P. Möller, J.R. Nix, W.D. Myers, and W.J. Świątecki, At. Data Nucl. Data Tables **59**, 185 (1995).
- [56] P. Moller, J. R. Nix, and K.-L. Kratz, At. Data Nucl. Data Tables **66**, 131 (1997).
- [57] G. Audi, A.H. Wapstra, and C. Thobault, Nucl. Phys A **729**, 337 (2003).

- [58] P. Möller *et al.*, Phys. Rev. C **79**, 064304 (2009).
- [59] N. Dubray and D. Regnier, Comp. Phys. Comm. **183**, 2035 (2012)
- [60] N. Schunck, D. Duke, H. Carr, and A. Knoll, Phys. Rev. C **90**, 054305 (2014).
- [61] V. Luc and P. Soille, IEEE Trans. Pattern Anal. Mach. Intell. **13**, 583 (1991).
- [62] A. Mamdouh, J.M. Pearson, M. Rayet, and F. Tondeur, Nucl. Phys. A **644**, 389 (1998).
- [63] B. Hayes, Am. Sci. **88**, 481 (2000).
- [64] P. Möller, A. J. Sierk and A. Iwamoto, Phys. Rev. Lett. **92**, 072501 (2004).
- [65] W. Brodziski, P. Jachimowicz, M. Kowal, and J. Skalski, "Superheavy Nuclei - Structure, High-K Ground States, Limits of Stability", JPS Conf. Proc. Vol. **6**, 020054 (2015), Proceedings of the Conference on Advances in Radioactive Isotope Science (ARIS2014).
- [66] A. Baran, M. Kowal, P.-G. Reinhard, L. M. Robledo, A. Staszczak, and M. Warda, Nuclear Physics A **944**, 442-470, (2015).
- [67] T. Cap, K. Siwek-Wilczynska, M. Kowal, and J. Wilczynski, Phys. Rev. C **88**, 037603 (2013).
- [68] K. Siwek-Wilczynska, T. Cap, M. Kowal, A. Sobiczewski, and J. Wilczynski, Phys. Rev. C **86**, 014611 (2012).
- [69] T. Cap, K. Siwek-Wilczynska, and J. Wilczynski, Phys. Rev. C **83**, 054602 (2011).
- [70] A. Rahmatinejad, A. N. Bezbakh, T.M. Shneidman, G.G. Adamian, N.V. Antonenko, P. Jachimowicz, and M. Kowal, (2020) unpublished.
- [71] G.G. Adamian *et al.*, Int. J. Mod. Phys. E **5**, 191 (1996).
- [72] M.G. Itkis, Yu.Ts. Oganessian, and V.I. Zagrebaev, Phys. Rev. C **65**, 044602 (2002).